Proceedings of the 5th International Conference on Computing and Data Science
DOI: 10.54254/2755-2721/13/20230713

Fractal analysis of rock pore structure: A comparative study of the Matlab-based image method and the mercury intrusion method

Xuying Zeng

Ocean University of China, Songling Road 238, Laoshan, Qingdao, Shandong, 266100

tzk1007@163.com

Abstract. As a naturally porous medium, rocks have a very strong heterogeneity in their internal pore structure, which has an important impact on the mechanical and chemical properties of rocks, etc. Therefore, it is very important to quantitatively characterise the heterogeneity of the pore structure of rocks. Fractal dimension has long been recognised as an effective means of characterising the heterogeneity of the pore structure of porous media and is widely used in oil and gas exploitation, construction materials, mining, and water engineering. There are different methods to calculate the fractal dimension. To verify the consistency between different methods, this paper compares the results of fractal analysis using the mercury intrusion method and MATLAB image fractal analysis using three rock samples with large differences in porosity and calculates the fractal dimension in three different ways on the basis of the mercury intrusion method. The results demonstrate that the fractal dimension of the mercury intrusion method and the box counting dimension of the image analysis obtained by the three methods, although slightly different in numerical value, are consistent in their numerical relationship, i.e., they all conform to the rule that the stronger the non-homogeneity of the pore throat, the larger the fractal dimension. The results of this paper show that fractal dimension is indeed an effective means of characterising rock homogeneity.

Keywords: rock pore structure, fractal dimension, image analysis, mercury intrusion.

1. Introduction

Porous structures are widely found in nature and engineering applications, such as the soil, rocks, bones, and trees that make up the Earth's biosphere, as well as pore materials including ceramics, metals, and organic materials, which are widely used in industrial processes such as construction, metallurgy, machinery, oil, and gas [1]. The results of previous studies show [2] that the porous structure is one of the key factors affecting the intrinsic characteristics and utilization of porous materials, and it is important to accurately characterize the pore structure of materials. For the quantitative description of the pore structure, the previous use of Euclidean geometry for the measurement of characteristic lengths or proportions no longer meets the realistic needs. Since the concept of fractal geometry was introduced by B.B. Mandelbrot in 1975, the concept has been used in a variety of fields, including applications in the pore structure of petroleum reservoirs. Tight oil and gas sandstone reservoirs are an important part of unconventional oil and gas reservoirs. Unlike

DOI: 10.54254/2755-2721/13/20230713

conventional sandstone reservoirs, tight sandstone extensively develops a micro- and nano-scale pore throat system, which is manifested by the narrow and non-homogeneous pore throat of the system and has important implications for the study of seepage characteristics and recovery effects of tight reservoirs [3-5]. The pore structure in a reservoir is closely related to the production and accumulation rate of hydrocarbons. Pore type, size, and arrangement can not only affect the reservoir and accumulation of hydrocarbons but also respond to the hydrocarbon reserves [6-7]. Therefore, quantitative characterisation of pore structure is necessary for hydrocarbon reservoirs, especially tight reservoirs, and previous studies have shown that fractal analysis is one of the effective tools that can help establish an evaluation method for the pore system of reservoir rocks.

Existing characterisation methods applied to pore structure mainly include mercury intrusion porosimetry (MIP), gas (CO2, N2, and water vapour) adsorption, nuclear magnetic resonance (NMR), CT scanning, and so on. Due to the limitations of the assay methods themselves and the heterogeneity of the rocks, the scales that can be observed by different technical methods do not reflect the overall characteristics of the reservoir and will yield different evaluation results [7], and therefore need to be analysed in conjunction with the evaluation results of different experiments. Therefore, in this study, the fractal dimension of the samples is obtained by using the mercury intrusion method and the image method based on the previous mercury intrusion data and CT images, and the differences between the two methods are compared to evaluate the effectiveness of the different fractal analysis methods. The validity of the different fractal analysis methods was evaluated.

2. Methods and Techniques

Fractal theory is a method for studying the internal structure of irregular forms based on their self-similarity. Previously, it was found that fractal theory is applicable to characterise the pore structure of complex lithologies such as sandstones, carbonate rocks, and mud shales. The complexity and irregularity of the reservoir pore structure can be quantitatively characterised using the fractal dimension D. The smaller the value, the more regular and less heterogeneous the pore shape is [8].

2.1. Analytical Method: Mercury Intrusion Method

The basic principle of using the high-pressure mercury injection method to study the pore distribution of rocks is that mercury in the non-wetting phase overcomes the capillary pressure in the pore throat to enter the pore throat; the higher the driving pressure, the higher the amount of incoming mercury and the smaller the corresponding radius [3]. The injection pressure can be converted into the corresponding pore throat radius according to the Young-Laplace equation.

$$P_c = \frac{2\sigma cos\theta}{r} \tag{1}$$

Where P_c is the capillary pressure; is σ surface tension (generally taken as 0.48 N/m). θ is the contact angle (140°). Then the imput mercury volume corresponding to the imput mercury pressure is the pore throat space corresponding to the corresponding pore throat radius, and the pore distribution characteristics can be obtained by plotting the capillary pressure curve.

The pore fractal dimension is calculated as:

$$D = \lim_{\varepsilon \to 0} \frac{logN(\varepsilon)}{log\left(\frac{1}{\varepsilon}\right)} \tag{2}$$

If the distribution of pore throat reservoir space within a rock conforms to the fractal character, the following relationship is satisfied:

$$N(r) \propto r^{-D} \tag{3}$$

The physical parameters in the formula are as follows: r is the radius of the pore-throat reservoir space,ε is the characteristic length, which corresponds to the radius of the pore throat in the storage

DOI: 10.54254/2755-2721/13/20230713

space, D is the corresponding fractal dimension of the pore throat storage space, and N(r) is the number of pore throat storage spaces with radius r

Combined with capillary models Equation 4 can be obtained:

$$N(r) = \frac{V_{Hg}}{\pi r^2 l} \tag{4}$$

where l is the length of the capillary tube and V_{Hg} is the total volume of mercury injected, then combining Eq.3 and Eq.4 gives:

$$\frac{V_{Hg}}{\pi r^2 l} \propto r^{-D} \tag{5}$$

Combining this with the capillary model gives:

$$V_{Hg} \propto r^{2-D} \tag{6}$$

Then the combination of Eq.1 gives:

$$V_{Hg} \propto {P_c}^{-(2-D)} \tag{7}$$

Since the mercury saturation is:

$$S_{Hg} = \frac{V_{Hg}}{V_p} \tag{8}$$

Where V_p is the pore volume, then:

$$S_{Hg} = \alpha {P_c}^{-(2-D)} \tag{9}$$

Further, by taking the derivative of both sides of the equation with respect to P_c:

$$\frac{dS_{Hg}}{dP_c} \propto {P_c}^{-(3-D)} \tag{10}$$

2.2. MATLAB-based Fractal Analysis

Experimental analysis images were obtained from samples 10560_1_HR4 (Sample 1, porosity 6.49%) by Christoper J. Landry [5] (Fig. 1), 77 (Sample 2, porosity 14.2%) by Gilbert Scott [9] (Fig. 2), and 44 (Sample 3, with a porosity of 28.3%) (Fig. 3). The graph shows that the greater the porosity, the more heterogeneous the sample.

For a strictly self-similar fractal, the following equation is available.

$$D_s = \frac{lnN}{ln\frac{1}{r}} \tag{11}$$

whereD_s is the similarity dimension, N is the number of similar elements, and r is the similarity ratio of similar elements. The counting box dimension, extended from Hausdorff dimension, is widely used in fractal analysis for curves and surfaces enclosed by curves and has little to do with the physical meaning of the image [10]. The calculation now binaries the image (Fig.4,5 and 6) and the figure is then covered with an equidistant square grid. After progressively refining the grid size, the number of box dimensions is calculated using the following formula [11].

$$D_B = lim\frac{lnN_{\delta_k}(F)}{-ln\delta_k} \tag{12}$$

whereN_{δ_k} is the number of δ_k-net cubes intersecting with F. The meaning of the formula is to divide the image into a grid whose side length is δ_k and then calculate the number of grids that cover the

DOI: 10.54254/2755-2721/13/20230713

region of interest in the image N_{δ_k}. If F has a fractal character, according to Eq.12, when $\delta_k \to 0, \frac{\ln N_{\delta_k}}{\ln \frac{1}{\delta_k}} \to D_B$, the fractal dimension can thus be found D_B. The lengths of the sides of the boxes taken for the three samples are δ_{k-1} =1, 2, 4 (sample1), δ_{k-2} =1, 4, 16 (sample2), and δ_{k-3} =1, 4, 16 (sample3).

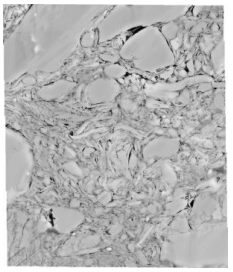

Figure 1. Sample 1.

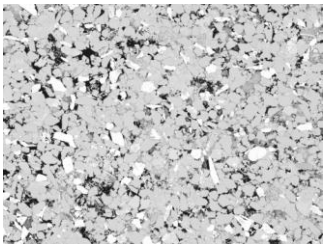

Figure 2. Sample 2.

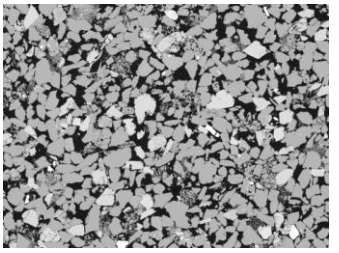

Figure 3. Sample 3.

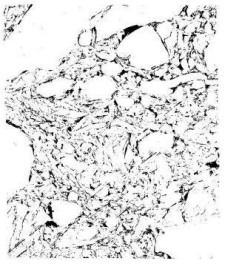

Figure 4. binary chart of sample 1.

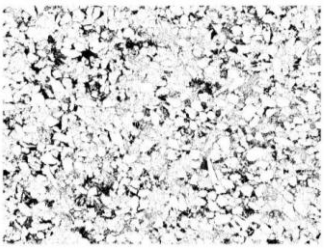

Figure 5. binary chart of sample 2.

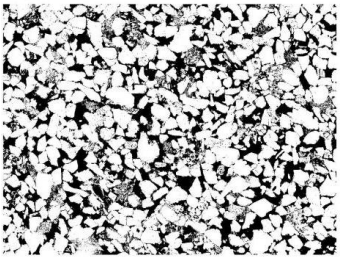

Figure 6. binary chart of sample 3.

Using image processing and numerical calculation functions in MATLAB, the image of the area of interest was extracted, and the CT scan image of the sample was binarized and converted into a black and white bitmap. And then the grayscale images were compared, and noise points with pixel values less than 4 were removed for subsequent extraction of image features. The colour value corresponding to each element in the digital image is stored in the corresponding position of the corresponding size matrix. According to the principle of box dimensions, the binary map is gridded and counted to obtain the number of grids covering the object area corresponding to the different grid edge lengths. The absolute value of the slope of the image is the boxed dimension when plotted in bilogarithmic coordinates D_B.

3. Results and Discussion

3.1. Calculation of the Fractal Dimension by the MIP Method

Experimental sample data were obtained from tight sandstone samples LD-1 and LD-8 in Ruilinag Guo, 2019 [12] and a core sample from an oil reservoir S2 in Kewen Li, 2004 [13]. The porosities of the three samples were 11.05% (LD-1), 3.08% (LD-8), and 26.32% (S-2). According to Eq. 3, 9, and 10, the homogeneity of the pores can be compared in three ways.

DOI: 10.54254/2755-2721/13/20230713

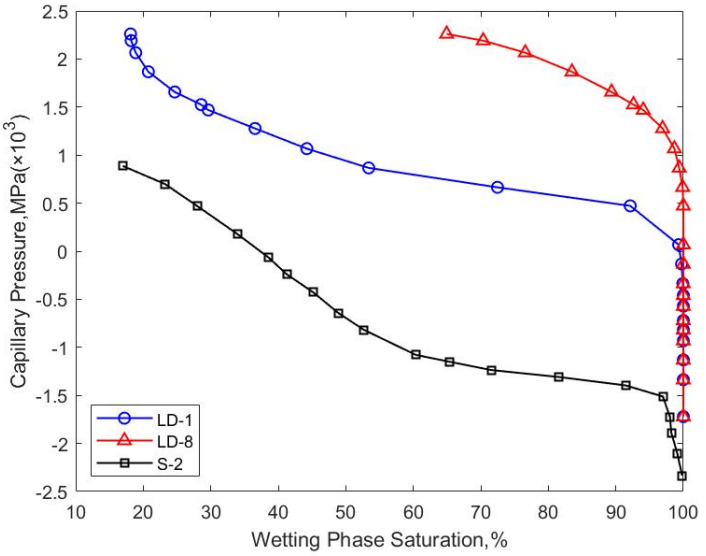

Figure 7. Capillary pressure curves of the three core samples from oil reservior.

Fig. 7 shows the capillary pressure curves for the three samples, with the wet phase saturation as the horizontal coordinate and the capillary pressure as the vertical coordinate, which can be used to determine the heterogeneity of the three samples. It is clear from the graph that the homogeneity varies very much between the three samples. Sample LD-8 was the most heterogeneous, and sample S-2 was the most homogeneous. Therefore, the heterogeneity of the three samples satisfies the following relationship.$D(LD-8) > D(LD-1) > D(S-2)$. i.e., the smaller the porosity, the larger the fractal dimension.

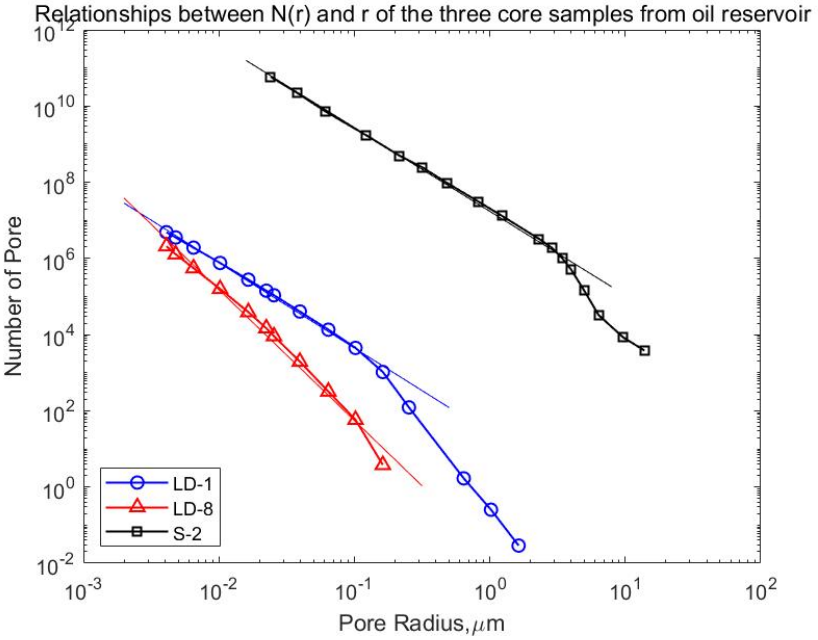

Figure 8. Relationships between N(r) and r of the three core samples from oil reservior.

DOI: 10.54254/2755-2721/13/20230713

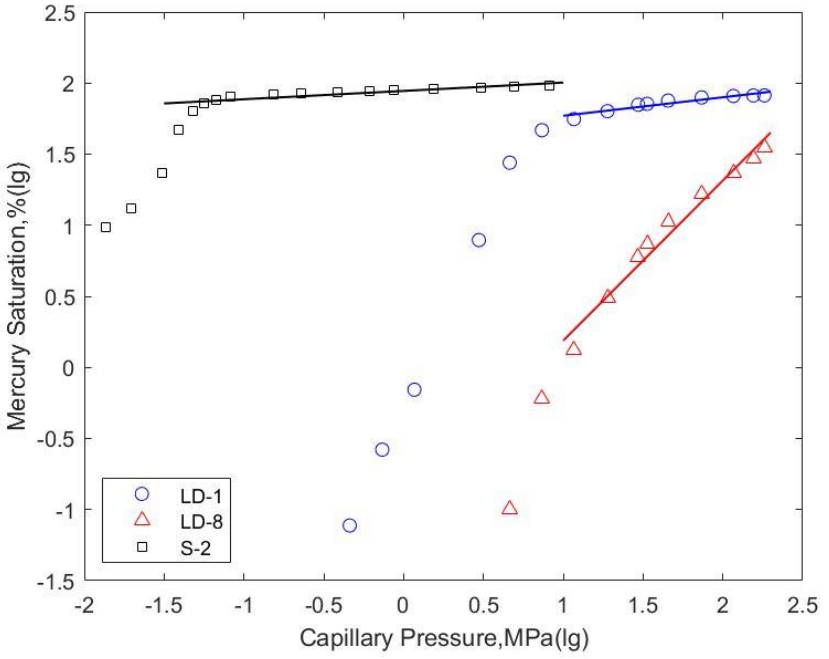

Figure 9. Capillary pressure curves of the three core samples from oil reservior.

Table 1. Fractal dimensions of the three samples obtained by different methods.

Sample	Method	LD-1	LD-8	S-2
D_B	Eq. 3	2.2373	3.4327	2.2011
	Eq. 9	2.1300	3.1264	2.0586
	Eq. 10	2.0248	3.1376	1.7380
Porosity		11.05%	3.08%	26.32%

From Fig. 8, calculated by Eq. 3, it can be seen that the radius of the pore throat and the number of pore throats of the corresponding radius are linear in a double logarithmic coordinate system. It can be seen from Eq. 2 that the pore throat system for all three samples is generally fractal and can be inscribed by fractal geometry, and that the slope of the one-dimensional fitted curve reflects the fractal dimension of the sample (Table 1). Based on the images, some of the data points for large pore radii deviate from the fitted straight line, indicating that the large radius pore throats may not be fractal. Based on the calculated results, the fractal dimension of these samples satisfies the relationship of $\mathrm{Df(LD-8)} > \mathrm{Df(LD-1)} > \mathrm{Df(S-2)}$, distributed between 2.9 and 3.5.

Fig. 9 shows a plot of mercury saturation versus capillary pressure based on Eq. 9. All three sample curves satisfy a linear relationship at capillary pressures above a certain value, and fractal dimension values can be calculated from the equation. (Table 1).

DOI: 10.54254/2755-2721/13/20230713

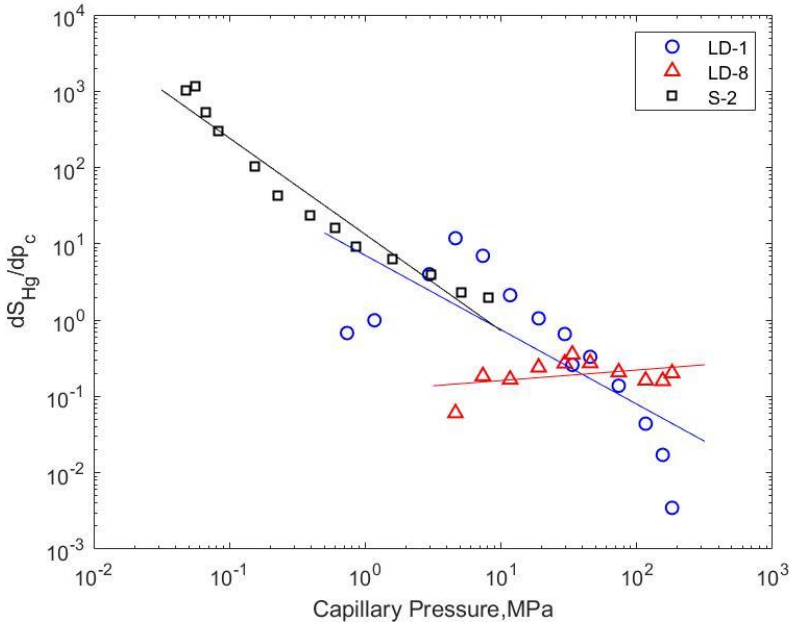

Figure. 10. Relationships between dS_{Hg}/dp_c and p_c of three core samples.

Fig. 10 is plotted according to Equation 11, with the data points more dispersed than in Figs. 8 and 9, and the resulting fractal dimension calculated according to the equation is shown in Table 1. Again, the heterogeneity of the three samples characterised by the fractal dimension obtained by this method still satisfies the relationship $\mathrm{Df(LD-8)} > \mathrm{Df(LD-1)} > \mathrm{Df(S-2)}$ and took values between 1.8 and 3.2, with a range that varied compared to the previous two.

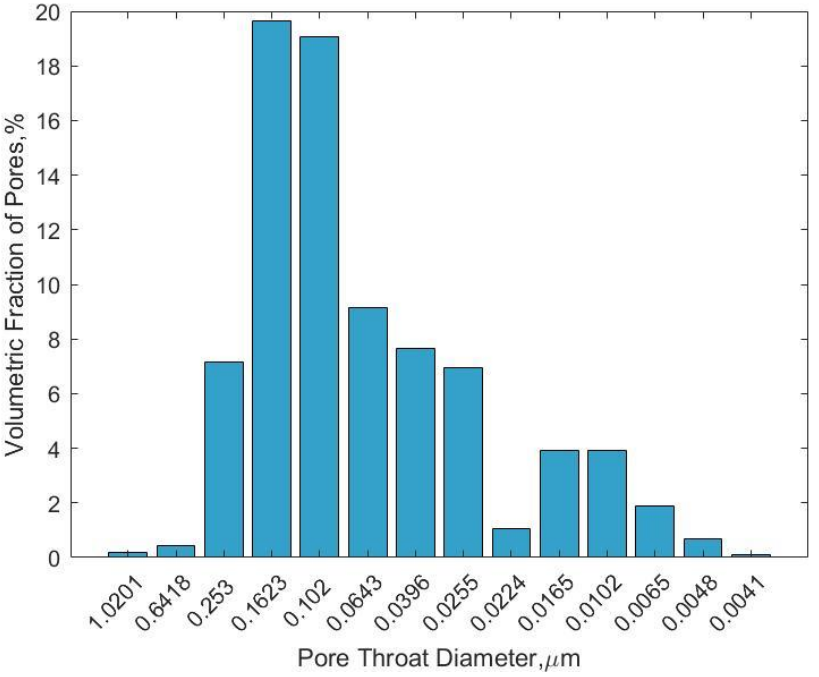

Figure 11. Pore size distribution of core LD-1.

DOI: 10.54254/2755-2721/13/20230713

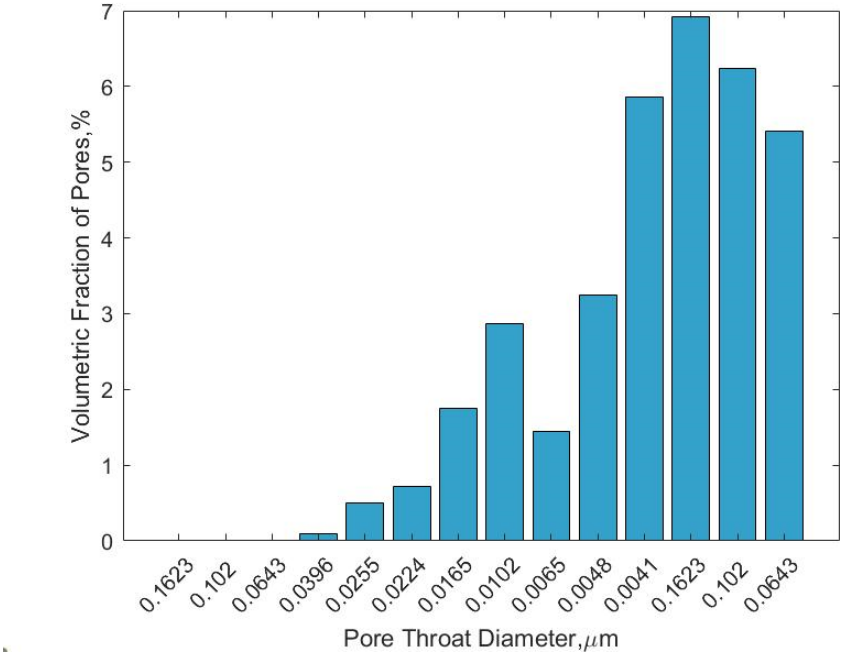

Figure 12. Pore size distribution of core LD-8.

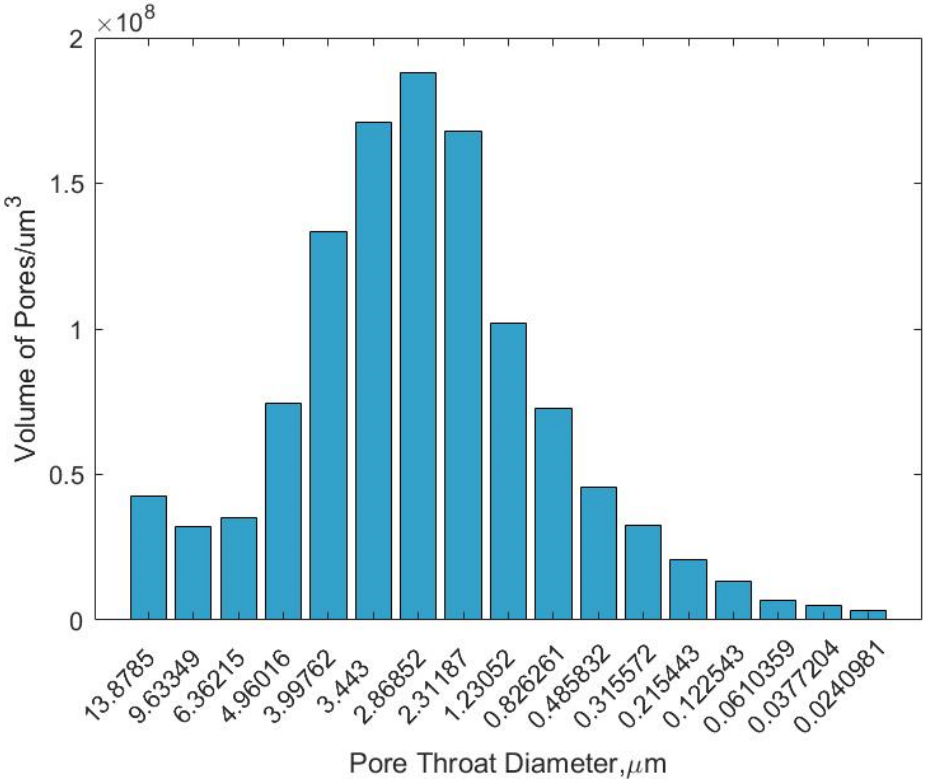

Figure 13. Pore size distribution of core S-2.

DOI: 10.54254/2755-2721/13/20230713

The pore throat size distribution, as characterised by the pore throat radius, is represented in Fig.11-13 and allows a more visual comparison of sample heterogeneity. As can be seen from the first two graphs, samples LD-1 and LD-8 have distinct double peaks, whereas sample S-2 has only one distinct peak, and this peak is relatively concentrated. So, it's clear that samples LD-1 and LD-8 are more different from each other than sample S-2, which is also what the numbers in Table 1 say.

3.2. Image Analysis to Calculate the Box Dimension

According to the steps as above, a double logarithmic image is made with the grid edge length L as the horizontal coordinate and the number of grid n (L) covering the image of interest as the vertical coordinate, and the result can be obtained as shown in Fig. 14. The absolute value of the slope of the fitted one-dimensional straight line is the counted box dimension of the calculated sample. $D_{B-sample1} = 0.5103, D_{B-sample2} = 1.3465, D_{B-sample3} = 1.5747$ Again, in accordance with the law, the smaller the porosity, the larger the fractal dimension.

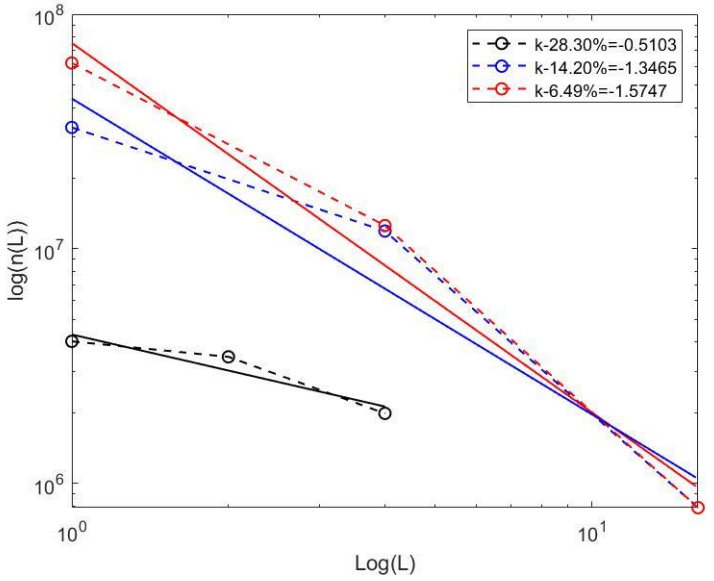

Figure 14. Fractal analysis.

4. Discussion

Fractal theory uses self-similarity to study the non-homogeneity of rocks and can quantitatively describe the complexity of pore structure for classification and evaluation purposes [5,14]. In this paper, using previous mercury intrusion data as well as rock CT scan images, two different methods, mercury intrusion fractal analysis and MATLAB image analysis, were used to obtain consistent results, indicating that both fractal dimensions are effective methods for characterising rock heterogeneity. As shown in Fig. 15, from the trend of fractal dimension obtained from the three calculation methods based on the mercury intrusion data and that of the box counting dimension derived from image analysis, it can be seen that the different methods satisfy the rule that the larger the porosity, the lower the pore structure inhomogeneity, and the smaller the fractal dimension, which is consistent with the previous studies [8,15-17].At the same time, according to the previous research results [18,19], this conclusion is also applicable to other porous media.

In three-dimensional Euclidean space, the fractal dimension of the pore structure is between 2 and 3. This is also the theoretical interval for the fractal dimension of the MIP method. While the fractal dimension of a two-dimensional plane is theoretically between 1 and 2, the larger the fractal dimension, the more the pores tend to fill the entire plane, i.e., the greater the heterogeneity [20] , and since the image method used in this paper is based on the analysis of two-dimensional images, the

DOI: 10.54254/2755-2721/13/20230713

theoretical value of the fractal dimension is between 1 and 2. Therefore, in this study, the fractal dimension obtained for MIP is generally greater than the box counting dimension(Fig. 15).

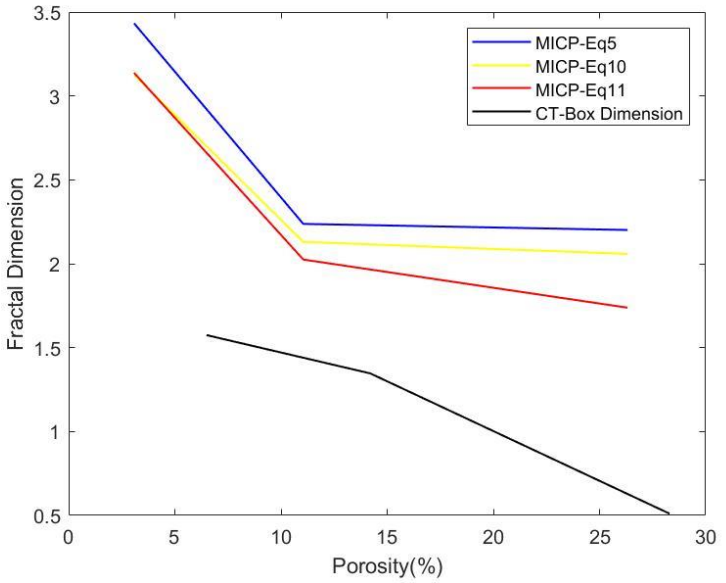

Figure 15. Comparison of different fractal analysis methods.

5. Conclusion

(1) The data obtained, whether using MIP or CT scan images, are consistent with the relationship that the greater the porosity, the more heterogeneous the reservoir.

(2) The fractal dimensions calculated by the different methods differ numerically but follow the same trend with porosity.

(3) The fractal dimension of the pore structure can better quantify the porosity, and there is a good correspondence between the size of the fractal dimension and its physical properties: the larger the porosity, the larger the fractal dimension. This is consistent with the results of previous studies.

References

[1] Zhu Jilei,Tang Huiping,Xi Zhengping,Di Xiaobo. Fractal Analysis of Pore Structure and Its Application for Prediction of Permeability and Porosity[J]. Rare metal materials and engineering,2009,38(12):2106-2110.

[2] Pandey S P, Sh arma R L. Cem Coner Res[J], 2000, 30(1):19.

[3] Zou Caineng, Zhu Rukai, Wu Songtao, Yang Zhi, Tao Shizhen, Yuan Xuanjun, Hou Lianhua, Yang Hua, Xu Chunchun, Li Denghua, Bai Bin, Wang Lan. Types, characteristics, genesis and prospects of conventional and unconventional hydrocarbon accumulations: taking tight oil and tight gas in China as an instance,[J].Acta Petrolei Sinica,2012,33(02):173-187.

[4] Wang Wei, Zhu Yu-shuang, Yu Cai-li, Zhao Le, and Chen Da-you. Pore size distribution of tight sandstone reservoir and their differential origin in Ordos Basin [J].Natural Gas Geoscience,2019,30(10):1439-1450.

[5] Wang Wei, Song Yuanjuan, Huang Jing, Li Yahui, Chen Zhaobing, Zhu Yushuang. Fractal characteristics of pore-throat structure in tight sandstones using high-pressure mercury instrusion porosimetry[J].Bulletin of Geological Science and Technology,2021,40(04):22-30+48.DOI:10.19509/j.cnki.dzkq.2021.0402.

[6] Zhu Z-Bao,Bai Y-Q. Fractal geometry and its applications[J]. Value Engineering,2012,31(35):5-7.

[7] Zou Caineng, Yang Zhi, Zhu Rukai, Zhang Guosheng, Hou Lianhua, Wu Songtao, Tao Shizhen, Yuan Xuanjun, Dong Dazhong, Wang Yuman, Wang Lan, Jinjin Liang, Wang Shufang. Petro China Research Institute of Petroleum Exploration & Development[J]. Acta Geologica Sinica,2015,89(06):979-1007.

[8] ZHAO Jing,HUANG Zhilong,ZHANG Jing Yuan,DENG Guangjun,XU Ma Guang. Pore Structure Fractal and Graded Evaluation in Tight Sandstone Reserviors: A Case Study of the Huangliu Formation in the Ledong Area, Yinggehai Basin[J/OL]. Acta Sedimentologica Sinica:1-19[2022-10-07].

[9] Comparison of Wireline Log and SEM Image-Based Measurements of Porosity in Overburden Shales, January 2020, American Association of Petroleum Geologists (AAPG), DOI: 10.15530/urtec-2020-3141.

[10] Scott, Gilbert; Wu, Kejian; Zhou, Yingfang (2019). Multi-scale Image-Based Pore Space Characterisation and Pore Network Generation: Case Study of a North Sea Sandstone Reservoir. transport in Porous Media, (), -. doi:10.1007/s11242-019-01309-8

[11] PENG Ruidong,XIE Heping,JU Yang. Computation of fractal dimension of two-dimensional digital images[J]. Journal of China University of Mining & Technology,2004(01):22-27.

[12] Ruiliang Guo, Qichao Xie, Xuefeng Qu, Meijuan Chu, Shutong Li, Dongxu Ma, Xiaofeng Ma, Fractal characteristics of pore-throat structure and permeability estimation of tight sandstone reservoirs: A case study of Chang 7 of the Upper Triassic Yanchang Formation in Longdong area, Ordos Basin, China, Journal of Petroleum Science and Engineering, Volume 184, 2020, 106555, ISSN 0920-4105

[13] Li, Kewen. "Characterization of Rock Heterogeneity Using Fractal Geometry." Paper presented at the SPE International Thermal Operations and Heavy Oil Symposium and Western Regional Meeting, Bakersfield, California, March 2004.

[14] Chen Cheng,Sun Yimei. Pore structure dimensioning of sandstones and its applications[J]. Acta Sedimentologica Sinica,1996(04):109-114.

[15] HUANG Huihui,TAN Jianhua,HE Yan,TANG Chao,YANG Bo,ZHAO Hu,LI Yaoyin. Quantitative characterization of the pore structure and evaluation and prediction on low porosity and low permeability reservoirs[J]. Coal Technology,2022,41(10):94-96.

[16] Lv Tianxue, Zhang Guoyi, Yi Lixin, Li Zhongli, Song Peng, Li Siqi. Pore structure and fractal characteristics of low-permeability reservoirs in the Songliao Basin[J]. Special oil and gas reservoirs,2022,29(01):59-65.

[17] Lu Zhendong, Liu Chenglin, Zang Qibiao, etal. Analysis of pore structure of tight sandstone by high pressure mercury injection combined with fractal theory: A case study of Heshui area in Ordos Basin[J].Bulletin of Geological Science and Technology,202*,4*(*):1-10.

[18] Wang Jinchang, Zhang Sai, Xu Jinglei. Study on Fractal Model of Fuel Cell Gas Diffusion Layer[J].Materials Reports,2022,36(13):28-33.

[19] Liu Guodong, Wang Chenxi, Fu Sijia, Gao Xiuan, Li Jing. Establishment and modification on fractal model of imbibition characteristics of ground calcium carbonate pigment for paper coating[J].China Pulp & Paper, 2021,40(12):39-49.

[20] WANG Yan,MA Yao,WANG Ruogu,CHEN Yongzhen,SUN Boya,LI Wenhou,WU Yue. Fractal study of micro-pore structure of tight sandstone reservoir[J]. Journal of Northwestern University (Natural Science Edition),2019,49(06):935-940.